*European Journal of Orthodontics* 23 (2001) 217–232 © 2001 European Orthodontic Society

# Cortical bone mineral density in asymmetrical mandibles: a three-dimensional quantitative computed tomography study

K. Maki*, A. J. Miller***, T. Okano**, D. Hatcher***, T. Yamaguchi*, H. Kobayashi* and Y. Shibasaki*

Departments of *Orthodontics and **Oral Radiology, Showa University, Tokyo, Japan and ***Department of Growth and Development, University of California, San Francisco, CA, USA

SUMMARY The three-dimensional distribution (3D) of the highest mineralized cortical bone was evaluated in 32 subjects between the ages of 8 and 30 years with asymmetrical mandibles using quantitative computed tomography (QCT). The geometrical distribution of the highest mineralized areas (>1250 mg/cm$^3$) representative of mandibular cortical bone was determined by 3D reconstruction of the images. The length of the mandible on each side was determined by defining a new linear measurement from the centre of the 3D reconstructed condyle to the midline of the symphysis as identified from a submental view. The cross-sectional areas of the masseter and medial pterygoid muscles were assessed from bilateral axial views through the middle of the muscles parallel to the Frankfort–Horizontal plane.

Comparison between the lengths of the two mandibular sides (right – left = mm) indicated a range of asymmetries with an equal number of subjects with the left and right mandible longer. Comparison of the area of highest mineralized cortical bone between the right and left sides (R/L) to the ratio of the mandibular length (R/L) showed a high correlation coefficient ($r$ = 0.629) suggesting that the shortest mandibular side had more highly mineralized bone. A comparison of the area of highest mineralized cortical bone between the right and left sides (R/L) to the ratio of cross-sectional areas of the muscles showed the highest correlation coefficient ($r$ = 0.724) with the ipsilateral masseter muscle. These findings indicate that asymmetrical mandibles are associated with asymmetrical distributions of the highest mineralized cortical bone and that this is age dependent.

## Introduction

Recent techniques with computed tomography (CT) have provided a method to not only assess the infrastructure, but to quantify the bone mineralization defined by quantitative computed tomography (QCT) (Carter and Hayes, 1976; Bentzen *et al*., 1987; Bhasin *et al*., 1988; Ruegsegger *et al*., 1988; Maki *et al*., 1989, 1997; Faulkner *et al*., 1991; Bouvier and Hylander, 1996). Computer programs provide an accurate method to reconstruct the entire mandible from the computer-based images. In a previous study, a new calibration phantom for applying QCT to the human craniomandibular skeleton based on CT scans was introduced (Maki *et al*., 1997). The inclusion of a calibrated phantom with each subject has provided a method to extend the CT measurement of attenuation coefficients (i.e. Hounsfield units) to a biologically significant measure of mineralization (i.e. hydroxyapatite). With this technique established, a second investigation has focused on the changes in cortical bone in the developing mandible, and the distinction in the rate of change among female and male subjects with normal, symmetrical mandibles (Maki *et al.,* 2000). In this present study, the focus is on the bilateral distribution of

the highest mineralized regions in the asymmetrical mandible. CT reconstruction of the mandible has extended into developing finite element models (FEM) that predict stresses within the mandible based on computer models that include muscle function (Maki *et al*., 1997). FEM have been developed based on various parameters by other investigators validating such models (Moss *et al*., 1985; Korioth *et al*., 1992). The QCT data provides one method of predicting stresses within the mandible and will build on this initial data defining the distribution of cortical bone mineralization.

## Subjects and methods

### *Study sample*

Thirty-two subjects (20 females and 12 males) between the ages of 8 and 30 years were studied with CT scanning (Table 1). The data was obtained and stored between 1990 and 1998

**Table 1** Morphological measures of the left and right mandible including the ramus and corpus lengths with both condylar and gonial angles.

| | | | 3D measurement | | | | | | | | | | |
|---|---|---|---|---|---|---|---|---|---|---|---|---|---|
| Patient | | | Left side | | | | | | | | | | |
| No. | Age (years) | Gender | Ramus length (mm) | | Corpus length (mm) | | Full length (mm) | | Condylar angle (°) | | Gonial angle (°) | | Short side |
| | | | Mean | SD | Mean | SD | Mean | SD | Mean | SD | Mean | SD | |
| 1 | 18.0 | F | 65.5 | 1.4 | 93.5 | 2.0 | 148.0 | 2.4 | 47.0 | 1.5 | 131.2 | 2.7 | Right |
| 2 | 18.0 | M | 70.2 | 1.5 | 100.0 | 1.9 | 146.4 | 1.9 | 54.2 | 1.2 | 120.5 | 3.1 | Left |
| 3 | 12.0 | F | 69.9 | 2.1 | 123.7 | 2.0 | 162.0 | 2.7 | 52.4 | 1.5 | 121.2 | 1.8 | Right |
| 4 | 11.0 | F | 53.5 | 1.9 | 88.3 | 1.8 | 131.4 | 1.8 | 54.1 | 1.7 | 124.2 | 2.9 | Left |
| 5 | 17.0 | F | 64.9 | 1.8 | 91.9 | 1.7 | 151.1 | 2.0 | 55.3 | 1.3 | 136.9 | 3.4 | Right |
| 6 | 8.0 | F | 43.0 | 2.1 | 87.7 | 1.7 | 122.4 | 1.4 | 61.5 | 1.4 | 130.4 | 2.0 | Left |
| 7 | 14.4 | M | 56.6 | 1.6 | 107.9 | 1.9 | 148.7 | 1.7 | 55.3 | 1.9 | 120.0 | 1.9 | Left |
| 8 | 13.0 | F | 52.2 | 2.0 | 89.5 | 1.2 | 129.0 | 1.9 | 51.5 | 1.2 | 122.5 | 2.6 | Left |
| 9 | 21.5 | F | 66.0 | 2.2 | 86.0 | 1.4 | 139.6 | 2.1 | 56.6 | 1.3 | 123.7 | 2.0 | Right |
| 10 | 8.2 | F | 54.9 | 2.4 | 81.9 | 1.0 | 127.5 | 2.0 | 58.5 | 1.5 | 130.0 | 2.7 | Left |
| 11 | 28.3 | M | 67.4 | 1.9 | 114.2 | 1.8 | 164.4 | 2.5 | 63.2 | 1.9 | 130.3 | 3.0 | Left |
| 12 | 19.5 | F | 60.4 | 1.5 | 104.5 | 1.0 | 152.8 | 1.5 | 48.8 | 1.2 | 137.2 | 2.1 | Right |
| 13 | 14.6 | M | 59.2 | 2.1 | 87.7 | 1.8 | 142.6 | 1.4 | 53.5 | 1.2 | 136.6 | 2.0 | Right |
| 14 | 23.4 | F | 63.2 | 1.8 | 100.4 | 2.0 | 147.0 | 1.9 | 63.4 | 2.0 | 134.4 | 1.9 | Left |
| 15 | 22.5 | F | 72.8 | 1.4 | 109.2 | 2.2 | 168.0 | 1.7 | 65.7 | 2.1 | 122.1 | 2.1 | Right |
| 16 | 14.5 | F | 59.9 | 0.9 | 104.7 | 1.5 | 154.0 | 1.1 | 44.2 | 1.3 | 128.2 | 2.1 | Right |
| 17 | 17.5 | F | 62.6 | 0.7 | 96.2 | 1.7 | 153.0 | 1.0 | 55.7 | 1.6 | 136.1 | 1.4 | Left |
| 18 | 16.9 | M | 54.2 | 0.9 | 106.2 | 2.0 | 141.4 | 1.9 | 66.8 | 1.8 | 114.5 | 2.7 | Left |
| 19 | 24.5 | F | 57.8 | 1.5 | 94.5 | 1.9 | 146.0 | 2.0 | 67.2 | 1.7 | 130.8 | 1.7 | Left |
| 20 | 14.1 | F | 72.0 | 1.6 | 98.5 | 1.0 | 159.0 | 1.1 | 69.9 | 1.7 | 125.2 | 2.9 | Right |
| 21 | 20.5 | F | 63.8 | 1.2 | 100.4 | 1.9 | 146.0 | 1.9 | 45.2 | 1.1 | 126.3 | 3.4 | Right |
| 22 | 23.4 | M | 92.0 | 2.6 | 97.0 | 1.5 | 146.0 | 3.4 | 72.8 | 1.8 | 128.0 | 4.3 | Left |
| 23 | 29.1 | M | 59.2 | 1.1 | 86.7 | 2.7 | 142.0 | 1.2 | 60.4 | 1.4 | 135.6 | 2.8 | Left |
| 24 | 24.0 | F | 61.0 | 2.4 | 104.7 | 2.8 | 157.0 | 3.4 | 61.1 | 1.7 | 127.0 | 3.7 | Right |
| 25 | 17.0 | F | 56.9 | 2.5 | 108.0 | 1.9 | 148.0 | 1.8 | 62.1 | 1.4 | 119.0 | 1.9 | Left |
| 26 | 15.4 | F | 60.4 | 2.5 | 104.5 | 2.6 | 151.0 | 2.4 | 68.3 | 1.3 | 137.2 | 3.6 | Left |
| 27 | 18.4 | M | 60.2 | 1.5 | 109.1 | 1.5 | 158.0 | 1.5 | 69.1 | 1.0 | 136.9 | 2.1 | Left |
| 28 | 21.0 | M | 70.1 | 1.8 | 124.5 | 1.8 | 164.0 | 1.8 | 51.7 | 1.0 | 122.0 | 4.3 | Right |
| 29 | 17.3 | M | 72.8 | 1.9 | 109.2 | 1.4 | 161.0 | 2.0 | 50.9 | 1.2 | 159.0 | 2.8 | Right |
| 30 | 23.5 | M | 60.4 | 0.6 | 105.0 | 1.3 | 154.0 | 1.9 | 51.2 | 1.0 | 136.0 | 3.4 | Right |
| 31 | 26.2 | F | 57.0 | 0.9 | 108.0 | 1.4 | 149.0 | 1.4 | 51.3 | 1.2 | 121.0 | 2.0 | Right |
| 32 | 23.0 | M | 58.0 | 0.8 | 87.0 | 0.9 | 144.0 | 1.3 | 61.2 | 1.7 | 135.0 | 3.3 | Left |

**Table 1** Continued

| Patient | | | 3D measurement | | | | | | | | | | |
|---|---|---|---|---|---|---|---|---|---|---|---|---|---|
| | | | Right side | | | | | | | | | | |
| No. | Age (years) | Gender | Ramus length (mm) | | Corpus length (mm) | | Full length (mm) | | Condylar angle (°) | | Gonial angle (°) | | Short side |
| | | | Mean | SD | Mean | SD | Mean | SD | Mean | SD | Mean | SD | |
| 1 | 18.0 | F | 57.1 | 2.0 | 104.4 | 2.0 | 136.0 | 2.4 | 61.3 | 1.6 | 126.8 | 3.0 | Right |
| 2 | 18.0 | M | 68.6 | 1.2 | 107.1 | 1.4 | 149.5 | 2.0 | 52.6 | 1.8 | 112.0 | 2.1 | Left |
| 3 | 12.0 | F | 73.6 | 1.7 | 120.8 | 1.9 | 158.0 | 2.3 | 56.3 | 1.3 | 115.9 | 2.2 | Right |
| 4 | 11.0 | F | 62.0 | 2.0 | 84.8 | 1.7 | 133.3 | 2.7 | 61.4 | 1.9 | 129.0 | 2.7 | Left |
| 5 | 17.0 | F | 63.6 | 1.0 | 92.4 | 1.1 | 143.1 | 2.1 | 57.4 | 1.5 | 134.0 | 3.6 | Right |
| 6 | 8.0 | F | 52.9 | 1.6 | 85.2 | 1.0 | 125.7 | 2.1 | 47.3 | 2.0 | 128.0 | 3.0 | Left |
| 7 | 14.4 | M | 68.6 | 1.2 | 100.4 | 1.9 | 154.0 | 2.0 | 53.4 | 1.4 | 114.1 | 2.9 | Left |
| 8 | 13.0 | F | 65.5 | 1.0 | 83.3 | 1.9 | 130.5 | 2.5 | 62.3 | 1.7 | 125.7 | 2.1 | Left |
| 9 | 21.5 | F | 66.9 | 1.5 | 88.1 | 1.2 | 136.3 | 2.0 | 61.4 | 1.4 | 121.0 | 3.2 | Right |
| 10 | 8.2 | F | 55.7 | 1.6 | 81.7 | 1.7 | 129.0 | 1.9 | 59.2 | 1.3 | 132.5 | 2.7 | Left |
| 11 | 28.3 | M | 84.8 | 1.5 | 111.5 | 1.5 | 171.7 | 1.9 | 56.3 | 1.2 | 126.3 | 2.1 | Left |
| 12 | 19.5 | F | 71.5 | 1.3 | 88.0 | 1.2 | 149.6 | 1.7 | 54.6 | 1.0 | 139.6 | 1.6 | Right |
| 13 | 14.6 | M | 48.3 | 1.4 | 99.6 | 1.7 | 135.6 | 2.0 | 58.3 | 1.2 | 136.3 | 2.7 | Right |
| 14 | 23.4 | F | 58.3 | 1.5 | 103.8 | 1.7 | 150.8 | 2.0 | 61.2 | 1.0 | 140.3 | 2.7 | Left |
| 15 | 22.5 | F | 82.1 | 2.1 | 106.0 | 2.2 | 157.0 | 1.9 | 62.4 | 1.2 | 129.1 | 2.1 | Right |
| 16 | 14.5 | F | 60.0 | 1.9 | 105.0 | 1.5 | 149.0 | 2.0 | 58.3 | 1.7 | 130.0 | 3.5 | Right |
| 17 | 17.5 | F | 60.2 | 1.5 | 109.1 | 1.8 | 158.4 | 1.9 | 54.6 | 1.9 | 136.9 | 2.4 | Left |
| 18 | 16.9 | M | 54.1 | 1.7 | 112.6 | 1.5 | 147.5 | 1.9 | 58.3 | 1.2 | 120.9 | 1.7 | Left |
| 19 | 24.5 | F | 59.2 | 1.9 | 94.3 | 1.8 | 155.9 | 1.5 | 61.3 | 1.3 | 138.7 | 2.0 | Left |
| 20 | 14.1 | F | 68.7 | 1.7 | 101.3 | 1.4 | 156.3 | 1.9 | 62.2 | 1.5 | 131.0 | 1.2 | Right |
| 21 | 20.5 | F | 59.4 | 1.9 | 85.9 | 1.0 | 131.0 | 2.1 | 58.3 | 1.9 | 127.6 | 1.9 | Right |
| 22 | 23.4 | M | 68.6 | 2.1 | 107.1 | 2.2 | 149.4 | 2.1 | 57.4 | 1.2 | 112.0 | 1.2 | Left |
| 23 | 29.1 | M | 79.0 | 1.2 | 113.0 | 1.9 | 162.6 | 3.5 | 59.2 | 1.2 | 160.0 | 4.7 | Left |
| 24 | 24.0 | F | 58.3 | 1.0 | 109.0 | 1.4 | 150.4 | 2.2 | 62.3 | 2.0 | 148.0 | 3.2 | Right |
| 25 | 17.0 | F | 69.0 | 1.0 | 123.0 | 1.2 | 164.0 | 1.8 | 61.3 | 2.1 | 121.0 | 2.4 | Left |
| 26 | 15.4 | F | 72.0 | 1.4 | 118.0 | 1.0 | 158.1 | 1.9 | 60.1 | 1.3 | 122.0 | 2.0 | Left |
| 27 | 18.4 | M | 80.0 | 1.3 | 112.0 | 1.7 | 168.0 | 2.1 | 64.3 | 1.6 | 158.0 | 1.9 | Left |
| 28 | 21.0 | M | 69.0 | 1.0 | 101.0 | 1.2 | 154.8 | 2.5 | 62.5 | 1.8 | 115.0 | 2.1 | Right |
| 29 | 17.3 | M | 67.0 | 1.8 | 100.4 | 2.0 | 154.9 | 2.7 | 51.4 | 1.9 | 114.1 | 2.9 | Right |
| 30 | 23.5 | M | 64.0 | 1.3 | 91.0 | 1.9 | 145.4 | 2.0 | 53.2 | 1.3 | 134.0 | 2.1 | Right |
| 31 | 26.2 | F | 64.0 | 1.3 | 94.0 | 1.5 | 144.0 | 1.9 | 54.9 | 2.3 | 136.0 | 3.3 | Right |
| 32 | 23.0 | M | 59.9 | 1.3 | 104.7 | 1.7 | 155.6 | 3.3 | 56.7 | 1.2 | 130.1 | 4.2 | Left |

at Showa University Medical Hospital and the Dental School. All subjects were referred for CT evaluation based on the presence of an asymmetrical mandible (i.e. >3-mm midline deviation) that had developed slowly over time during the pre-adolescent and adolescent years. Medical and dental history completed by individual interview of the subject and parent/guardian indicated no family history of an asymmetrical mandible, and a gradual development in the subject of this study. Informed consent for participation of each subject was obtained from the patient and/or parent/guardian. The study received approval from the Showa University Ethics Committee.

### *CT protocol*

A method was applied that was introduced in a previous study for obtaining images with a calibrated phantom, and then developing a three-dimensional (3D) reconstruction of the

mandible to determine the distribution of different levels of bone mineral density (Maki *et al*., 1997). This method includes a reference phantom. It has five rods containing calcium hydroxyapatite (HA), with different percentages as determined by weight: 112.9 (10 per cent), 174.9 (15 per cent), 241.3 (20 per cent), 312.5 (25 per cent), and 388.9 (30 per cent) mg/cm$^3$, respectively. The calibration phantom was positioned next to the head of each subject so both were scanned simultaneously. The CT measurements from the phantom were completed daily to determine reproducibility. The values varied from 3.0 to 4.0 per cent. The scanning axial image plane was determined by first obtaining a full head lateral scan (i.e. scout or scannogram) to visualize the Frankfort–Horizontal (FH) plane and then making all images parallel to this plane. Contiguous 2.0-mm thick slices were obtained through the entire mandible. Scanning parameters were set at 120 kVp, 60 mA, 3.0 seconds with a 180-mm field of view (FOV) and 512 × 512 pixels (Hitachi, W-600 scanner, Tokyo, Japan, and Yokogawa, Quantex scanner, Tokyo, Japan). Original data was stored on magnetic tape. All data, including run-length, was transmitted to a personal computer system (IBM PC) for transforming the data into a format for off-line analysis. The PC system was used to determine the mineral density. The attenuation values from the five-step phantom were transformed into HA values (mg/cm$^3$) and then each pixel attenuation value from the mandible was interpreted as mineral density.

3D bone measurements were developed from 3D reconstructed images using a workstation and supporting software (Voxel Flinger, Reality Imaging Corporation, Solon, Ohio, USA). This program allowed reconstruction of 3D images from voxels. The program also allowed removing overlying tissue and phantoms to unmask regions such as the condyle (Figure 1). The reconstructed

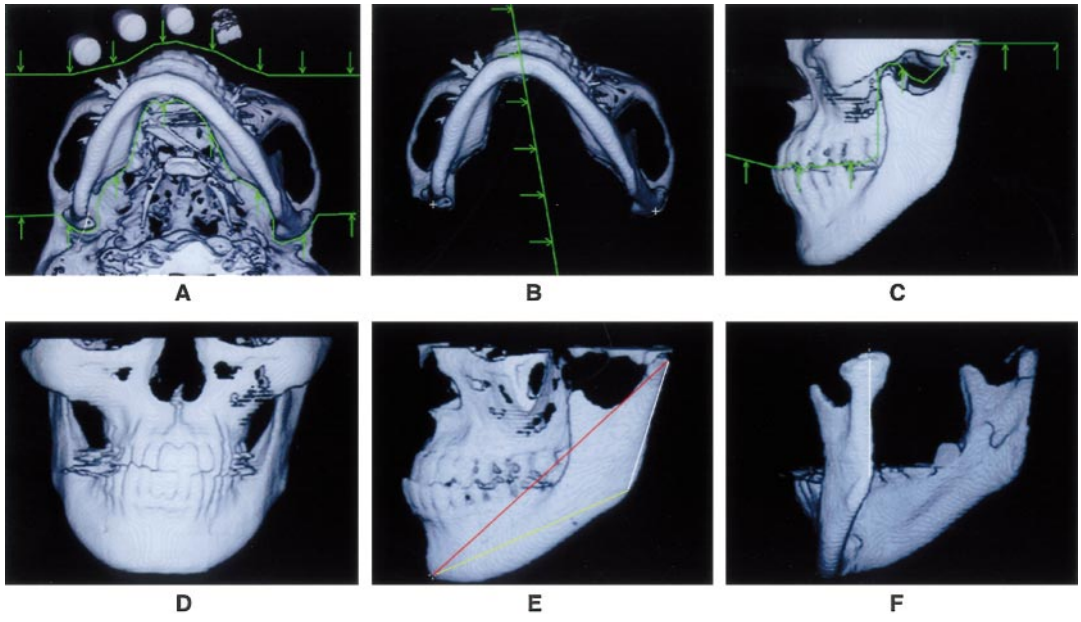


**Figure 1** A 3D reconstruction of the asymmetrical mandible in one subject with submental (A,B), lateral (C,E), frontal (D), and posterior (F), views. The 3D reconstructed image was based on originally acquired CT axial images. Software analysis allowed removal of sections (A, green arrows pointing toward retained structure) and retention of areas of interest (B, submental view). The mandible could also be separated (C, green line depicts separation site) from the rest of the craniomandibular skeleton. The method of determining the length of the right and left mandible involved defining the centre of each condyle, and projecting a line from the centre of the condyle to the most anterior point on the submental view of the mandible (B). The vertex of the gonial angle was determined from a lateral view (E) and the length of the ramus from a posterior view (F).

images were then evaluated from three different angles to determine a point (Figure 2). The points were determined independently by two investigators, and the length and angle determined for three repeated measures to obtain a mean value.

The muscle areas were determined using off-line analysis with customed-designed software (Voxel-View, Vital Images, Fairfield, Iowa, USA) on a Macintosh personal computer (Macintosh 8500, Apple Computer, Inc., Cupertino, California, USA).

*Mandibular length*

Five points were identified on the 3D reconstructed image with cut-aways of unnecessary tissue or calibrated phantoms (Figure 1). The five points selected were: the middle point on the posterior surface of the condylar head (Cd–R, Cd–L; Figure 1B); the most anterior point of the mandible (Pog; Figure 1B); and the vertex of the gonial angle (Go–R, Go–L; Figure 1E). Three lengths were then determined bilaterally: the full length of the mandible (Cd–Pog, Figure 1E); the length of the ramus (Cd–Go; Figure 1E, 1F); and the length of the mandibular corpus (Go–Pog, Figure 1E). Two angles were determined bilaterally: the gonial angle (Cd–R to Go–R to Pog; Cd–L to Go–L to Pog, Figure 1E); and the condylar angle (left condylar angle is Cd–L to Cd–R to Pog; right condylar angle is Cd–R to Cd–L to Pog; Figure 2). The 3D measurement for the length of the mandible was a linear distance from the most posterior centre of the condyle to the most anterior point of the mandible as defined in 3D space (Figure 2).

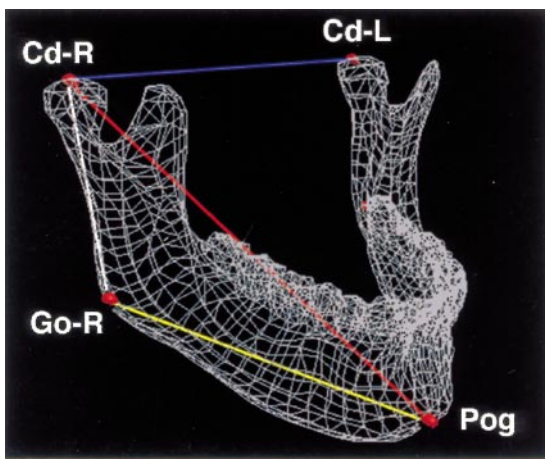


**Figure 2** The linear and angular measurements were determined after defining the centre of the condyle (Cd–R, Cd–L), the vertex of the gonial angle (Go–R), and the anterior point of the chin (Pog) on the 3D reconstructed images. The actual distances for the length of the ramus, mandibular corpus, and total mandibular length are determined in 3D space. The relationship of the 3D linear measures to the mandible are shown on a voxel-view display.

*Masseter and medial pterygoid cross-sectional areas*

The cross-sectional areas of the masseter and medial pterygoid muscles were evaluated by combining several axial views ($n$ = 10) through the middle of the muscles in a plane parallel to the FH plane. The cross-sectional area was measured from each axial view by counting the number of pixels that occupied the muscle. The initial scan was set at parameters ideal for viewing bone. Off-line analysis with contrast permitted identification of muscles and outlining their borders (Figure 3). Each pixel was a known size (0.350 × 0.350-mm) allowing a method to determine cross-sectional area by multiplying by the number of pixels in an area (Table 2). In each of the 10 axial views of a muscle, the muscle was outlined by hand. The middle of the muscles was chosen for analysis as this was the clearest region to identify the two muscles from other tissue in the CT scan (Figure 4). Anterior, posterior, and lateral views of the 3D reconstructed mandible provided a method to locate the level of analysis. The medial pterygoid muscle was the most difficult to evaluate as its direction of orientation at its insertion was difficult to distinguish from other muscles (i.e. lateral pterygoid) in that region.

*Cortical bone mineralization*

The total number of voxels for the mandible was displayed as mineralization levels from around 700 to 1700 mg/cm$^3$, with the range varying for each subject. The voxels with mineralization values exceeding the segmentation value around

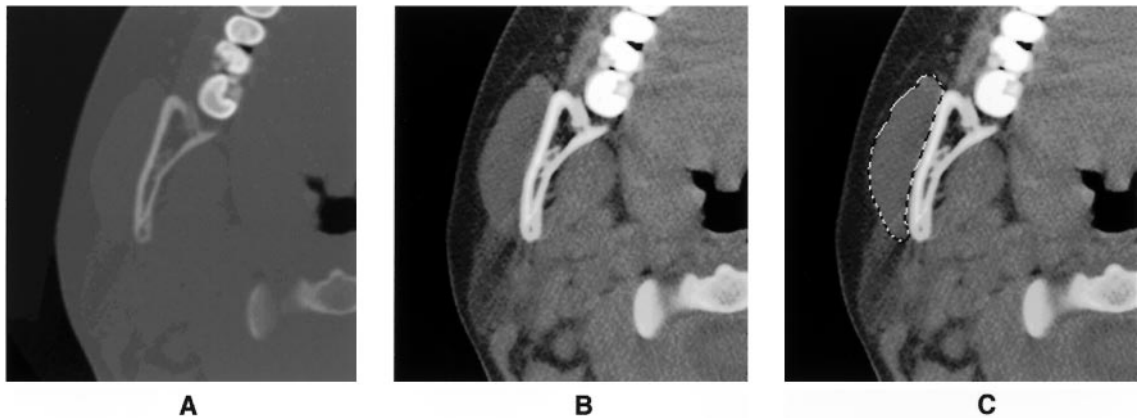


**Figure 3** An axial CT image of the mandible through the occlusal plane of one subject depicted at two different settings to show bone (A) and soft tissue (B,C). The outlined area (C) depicts the right masseter muscle and its cross-sectional area.

**Table 2** Size of the left and right masseter and medial pterygoid muscles as determined by the number of CT pixels and the cross-sectional area ($cm^2$).

| Patient | | | Masseter area (no. pixels) | | | | Medial pterygoid area (no. pixels) | | | | Masseter cross-sectional area ($cm^2$) | | Medial pterygoid cross-sectional area ($cm^2$) | |
|---|---|---|---|---|---|---|---|---|---|---|---|---|---|---|
| No. | Age (years) | Gender | Left mean | SD | Right mean | SD | Left mean | SD | Right mean | SD | Left | Right | Left | Right |
| 1 | 18.0 | F | 3245 | 26 | 3885 | 31 | 2701 | 32 | 1983 | 26 | 3.98 | 4.76 | 3.31 | 2.43 |
| 2 | 18.0 | M | 6115 | 31 | 5415 | 40 | 4243 | 25 | 3747 | 37 | 7.49 | 6.63 | 5.20 | 4.59 |
| 3 | 12.0 | F | 3410 | 29 | 3098 | 29 | 2481 | 30 | 2601 | 31 | 4.18 | 3.80 | 3.04 | 3.19 |
| 4 | 11.0 | F | 1614 | 19 | 1650 | 21 | 1589 | 22 | 1413 | 16 | 1.98 | 2.02 | 1.95 | 1.73 |
| 5 | 17.0 | F | 2440 | 21 | 3220 | 23 | 1524 | 22 | 1648 | 20 | 2.99 | 3.94 | 1.87 | 2.02 |
| 6 | 8.0 | F | 1920 | 22 | 2006 | 19 | 1770 | 19 | 1678 | 23 | 2.35 | 2.46 | 2.17 | 2.06 |
| 7 | 14.4 | M | 2115 | 29 | 2364 | 32 | 1770 | 19 | 1678 | 23 | 2.59 | 2.90 | 2.17 | 2.06 |
| 8 | 13.0 | M | 2035 | 26 | 2635 | 36 | 1745 | 26 | 2005 | 37 | 2.49 | 3.23 | 2.14 | 2.46 |
| 9 | 21.5 | F | 3099 | 37 | 3627 | 40 | 2632 | 37 | 2239 | 31 | 3.80 | 4.44 | 3.22 | 2.74 |
| 10 | 8.2 | F | 1754 | 15 | 1694 | 21 | 1605 | 34 | 1578 | 29 | 2.15 | 2.08 | 1.97 | 1.93 |
| 11 | 28.3 | M | 3369 | 27 | 2968 | 18 | 1862 | 21 | 2253 | 22 | 4.13 | 3.64 | 2.28 | 2.76 |
| 12 | 19.5 | F | 1738 | 29 | 2114 | 23 | 1673 | 20 | 1283 | 20 | 2.13 | 2.59 | 2.05 | 1.57 |
| 13 | 14.6 | F | 1550 | 19 | 2350 | 27 | 1804 | 23 | 1929 | 39 | 1.90 | 2.88 | 2.21 | 2.36 |
| 14 | 23.4 | F | 2917 | 26 | 3317 | 31 | 2466 | 21 | 2534 | 33 | 3.57 | 4.06 | 3.02 | 3.10 |
| 15 | 22.5 | F | 3227 | 37 | 2889 | 33 | 2504 | 36 | 2288 | 32 | 3.95 | 3.54 | 3.07 | 2.80 |
| 16 | 14.5 | F | 2651 | 31 | 2980 | 26 | 2250 | 29 | 2156 | 22 | 3.25 | 3.65 | 2.76 | 2.64 |
| 17 | 17.5 | F | 2660 | 29 | 2323 | 41 | 2085 | 20 | 1868 | 19 | 3.26 | 2.85 | 2.55 | 2.29 |
| 18 | 16.9 | M | 3115 | 31 | 2980 | 26 | 2250 | 29 | 2156 | 22 | 3.25 | 3.65 | 2.76 | 2.64 |
| 19 | 24.5 | F | 2482 | 20 | 2884 | 29 | 1466 | 22 | 1846 | 20 | 3.04 | 3.53 | 1.80 | 2.26 |
| 20 | 14.1 | F | 3654 | 39 | 2890 | 26 | 2005 | 31 | 2105 | 39 | 4.48 | 3.54 | 2.46 | 2.58 |
| 21 | 20.5 | F | 3560 | 40 | 3840 | 36 | 2330 | 26 | 2581 | 40 | 4.36 | 4.70 | 2.85 | 3.16 |
| 22 | 23.4 | M | 3651 | 18 | 3541 | 26 | 1406 | 21 | 1665 | 27 | 4.47 | 4.34 | 1.72 | 2.04 |
| 23 | 29.1 | M | 2650 | 22 | 2950 | 29 | 2113 | 29 | 2330 | 22 | 3.25 | 3.61 | 2.59 | 2.85 |
| 24 | 24.0 | F | 3105 | 39 | 3850 | 42 | 2420 | 31 | 2627 | 26 | 3.80 | 4.72 | 2.96 | 3.22 |
| 25 | 17.0 | F | 3880 | 28 | 3304 | 30 | 2740 | 29 | 2856 | 41 | 4.75 | 4.05 | 3.36 | 3.50 |
| 26 | 15.4 | F | 3010 | 29 | 3160 | 31 | 2110 | 29 | 2215 | 29 | 3.69 | 3.87 | 2.58 | 2.71 |
| 27 | 18.4 | M | 2510 | 15 | 2315 | 16 | 2105 | 36 | 2004 | 36 | 3.07 | 2.84 | 2.58 | 2.45 |
| 28 | 21.0 | M | 2540 | 25 | 2450 | 22 | 2105 | 36 | 2004 | – | 3.11 | 3.00 | 2.58 | 2.45 |
| 29 | 17.3 | M | 2450 | 22 | 3062 | 27 | 2004 | 26 | 2330 | 26 | 3.00 | 3.75 | 2.45 | 2.85 |
| 30 | 23.5 | M | 2880 | 19 | 2760 | 16 | 2340 | 35 | 2510 | 29 | 3.53 | 3.38 | 2.87 | 3.07 |
| 31 | 26.2 | F | 3540 | 40 | 3121 | 33 | 2554 | 31 | 2745 | 42 | 4.46 | 3.82 | 3.13 | 3.36 |
| 32 | 23.0 | M | 3350 | 32 | 2712 | 24 | 2815 | 29 | 2514 | 30 | 4.10 | 3.32 | 3.45 | 3.08 |

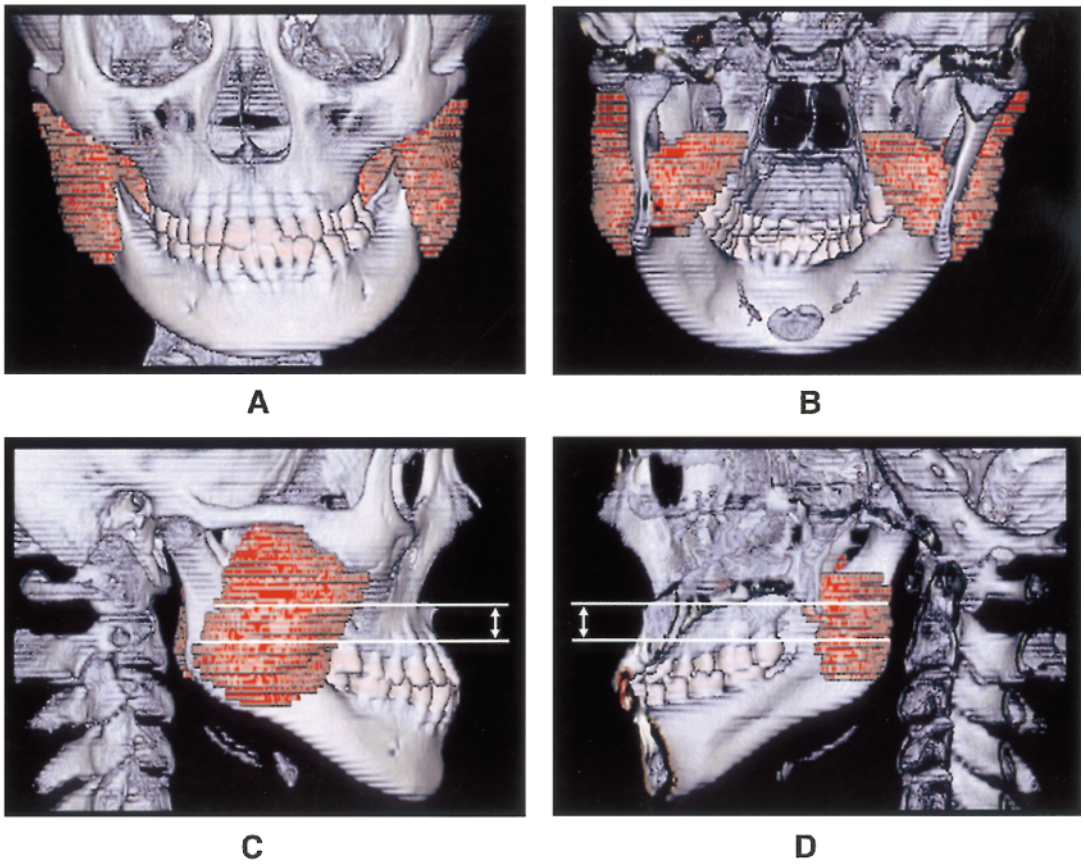


**Figure 4** 3D reconstructed views of the masseter and medial pterygoid muscles in one subject from the frontal (A), posterior (B), right lateral (C), and right medial (D) positions. The masseter and medial pterygoid muscles are depicted in red. The actual cross-sectional area measurements of both the right and left masseter and medial pterygoid muscles included 10 axial views through the belly of the muscles. The section of the muscles used to obtain the axial views for determining cross-sectional areas are shown between the two white lines in the two lower views (C,D). The plane of orientation for the muscle axial views was parallel to the FH plane. Note that the medial pterygoid muscle is not completely determined in its rostral region due to the difficulty in distinguishing it from surrounding muscles.

700 mg/cm$^3$ of HA defined the mandible, and included both cortical and some trabecular bone. The highest number of voxels occurred between 700 and 1100 mg/cm$^3$ of HA with a steady decline after that level. Above 1400 mg/cm$^3$ of HA, all subjects demonstrated a minimal number of voxels that extended to 1700 mg/cm$^3$ of HA. The PC software reconstructed the entire mandible and zygomatic arch. The 3D reconstructed mandible could be evaluated from any view, and was first reconstructed to obtain a lateral view of the right and then the left mandible, followed by a frontal and a submental vertex view. Successive sagittal sections were used to depict the entire condyle. Successive posterior views were used to show the direction and extend of the medial pterygoid muscle. Lateral views were used to identify the masseter muscle (Figure 4).

### *Highest cortical bone mineralization*

The cortical bone voxels with values exceeding 1250 mg/cm$^3$ were used to locate the highest mineralized cortical bone of the mandible. The individual horizontal images were integrated into a 3D reconstructed mandible to evaluate a frontal and two lateral views (Figure 5; right, left). The 3D program allowed depiction of selected levels of the mandible based on its mineralization level.

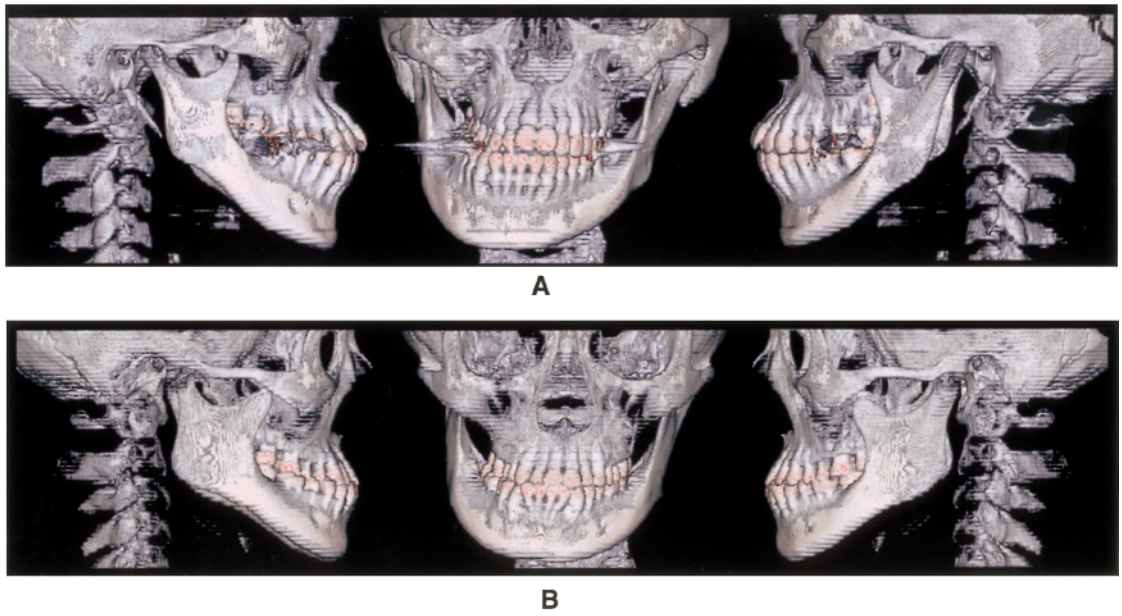


**Figure 5** Examples of the distribution of the highest mineralized cortical bone in the 3D reconstructed mandibles of two patients (A,B). Three views are presented: a frontal and two lateral views. The highest mineralized cortical bone (>1250 mg/cm$^3$) is shown in red. The bilateral distributions of the highest mineralized bone could be asymmetrical (A) or symmetrical (B). The total number of voxels on each side with highest mineralized cortical bone were determined and compared.

*Statistical analysis*

Comparison of several parameters between the right and left mandibular sides was completed by two methods. The first method subtracted the left from the right (R–L) for mandibular length, the number of pixels depicting the highest mineralized cortical bone, and the areas of the masseter and medial pterygoid muscles. In the second method, linear regression analysis was used to compare the ratio (R/L) of the number of pixels with highest mineralization on the right and left sides (R/L) to the ratios of several parameters: the right and left mandibular length, the masseter and medial pterygoid cross-sectional areas, and a combination of the masseter and medial pterygoid cross-sectional areas. Correlation coefficients (*r*-values) were used to determine the level of low to strong association. The percentage differences for the highest mineralized cortical bone between the right and left mandibular sides (R – L/R + L × %) was determined for three different age groups (8–14, 15–22, 23–30 years), and expressed as mean ± 1 SD and compared by a single factorial ANOVA. A *post hoc* Fisher analysis evaluated the data statistically with a $P < 0.05$.

## Results

*Mandibular length*

Comparison of the length between the right and left sides of the mandible (R – L = mm) indicated an equal distribution of subjects with left or right shorter sides (Figure 6A). Subjects ranged from mild asymmetry (3 mm) to extreme asymmetry (17–21 mm). Linear evaluations of the ramal length and corpus length of both sides indicated that the differences in mandibular length depended upon differences in either or both the mandibular corpus and the ramus (Table 1).

*Highest mineralized cortical bone*

Comparing the number of pixels that depicted cortical bone with mineralization >1250 mg/cm$^3$ between the right and left sides (R–L)

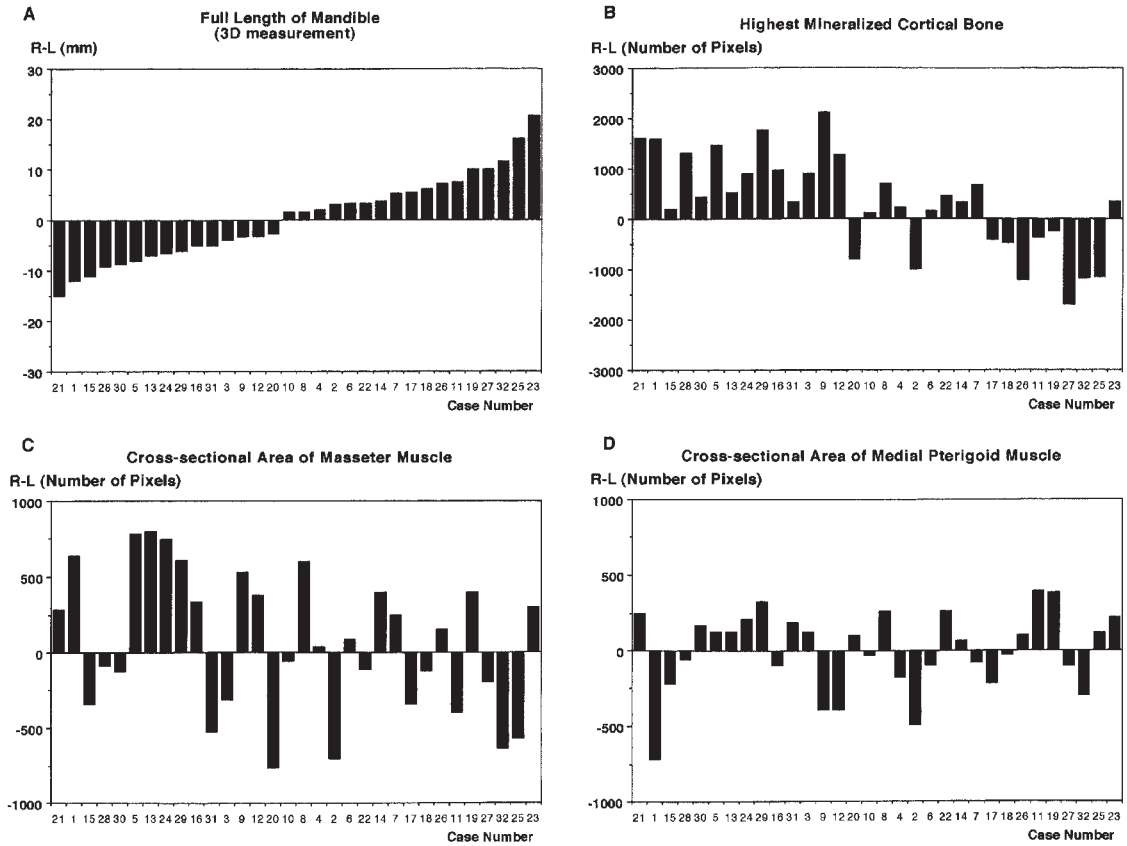


**Figure 6** The difference between the right and left sides (R–L) in the length of the mandible (A), the number of pixels for the highest mineralized cortical bone (B, >1250 mg/cm$^3$), the cross-sectional area of the masseter muscle (C, number of pixels), and the cross-sectional area of the medial pterygoid muscle (D, number of pixels) are shown for each of the subjects. All four graphs depict the same order of patients as shown in (A). Subjects with a shorter right mandible are shown on the left side of (A) and those with a shorter left side on the right.

demonstrated that almost all subjects with a shorter right side had a higher number of highest mineralized pixels on that side (Figure 6A and B). A majority of subjects with a shorter left side also demonstrated also demonstrated more pixels with the highest mineralized cortical bone. Evaluating the right and left differences in the number of pixels with the highest mineralized bone by ratio (R/L) to the mandibular asymmetries defined by the ratio (R/L) of the full length of the mandible showed a negative linear regression (Figure 7A; $r = 0.629$). The shortest mandibular side had more pixels and area with the highest mineralized cortical bone than the longer side. Comparing female to male showed a similar negative regression curve (male: $r = 0.489$, female: $r = 0.671$).

The percentage difference in this mineralized distribution between the right and left sides ($R - L/R + L \times \%$) changed with age (Figure 8A). The percentage difference in the number of highest mineralized pixels for a group of subjects with symmetrical mandibles is shown as the mean and one SD (Figure 8B). The subjects with asymmetrical mandibles demonstrated marked asymmetries in the amount of mineralization between the bilateral mandibular sides with the greatest changes between 15 and 23 years of age. Dividing the subjects with asymmetrical mandibles into three age groups with 7 years in

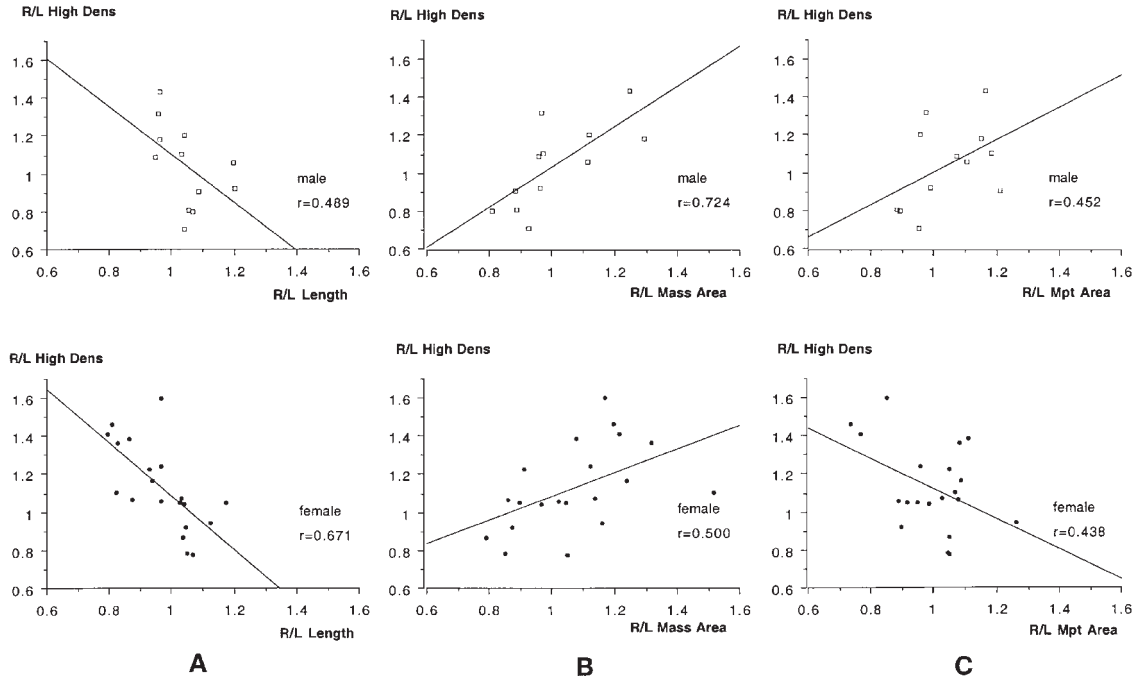


**Figure 7** The ratio between the right and left sides in the number of pixels with the highest mineralized bone (R/L High Dens) is compared with the ratio of mandibular length (A, R/L Length), masseter cross-sectional area (B, R/L Mass Area), and medial pterygoid cross-sectional area (C, R/L MPt Area). The data for both females (dark circles) and males (open squares) is shown.

each group (Figure 8B) showed that the subjects between the ages of 15–23 had a significantly higher asymmetry in the amount of highest mineralized cortical bone than the younger and older age groups (ANOVA, $P < 0.05$).

### *Masseter and medial pterygoid cross-sectional areas*

Subjects with the asymmetrical mandibles exhibited differences in the sizes of the bilateral masseter muscles (Table 2; Figure 6C). Some bilateral differences were shown in the medial pterygoid muscles, but those were not as pronounced (Figure 6D). Evaluating the gender of the subjects indicated that the females and males had similar sizes of muscles based on mean ± SD values (left masseter: female 3.40 ± 0.91, male 3.86 ± 0.38; right masseter: female 3.56 ± 0.84, male 3.69 ± 1.02; left medial pterygoid: female 2.62 ± 0.52, male 2.75 ± 0.89; right medial pterygoid: female 2.58 ± 0.56, male 2.80 ± 0.67). Comparison of the ratio of the number of pixels of the right masseter/left masseter (R/L mass) to the ratio of the number of pixels depicting the highest mineralized cortical bone of the right mandible to left (R/L) by linear regression indicated a strong correlation coefficient for both males and females (Figure 7B, male: $r = 0.728$; female $r = 0.500$). The larger the masseter muscle, the more regions of the ipsilateral mandible with the highest levels of mineralized cortical bone. An analysis of the ratio of the number of pixels for the medial pterygoid muscle size (R/L MPt) to the ratio of the number of pixels of highest mineralized cortical bone (R/L) indicated a positive correlation for the male (Figure 7C; male: $r = 0.452$) and a negative correlation for the female (female: $r = -0.438$). The correlations were relatively weak for comparison of the size of the medial pterygoid and the extent of development of the highest mineralized mandibular cortical bone. Combining the right masseter and medial pterygoid muscles and

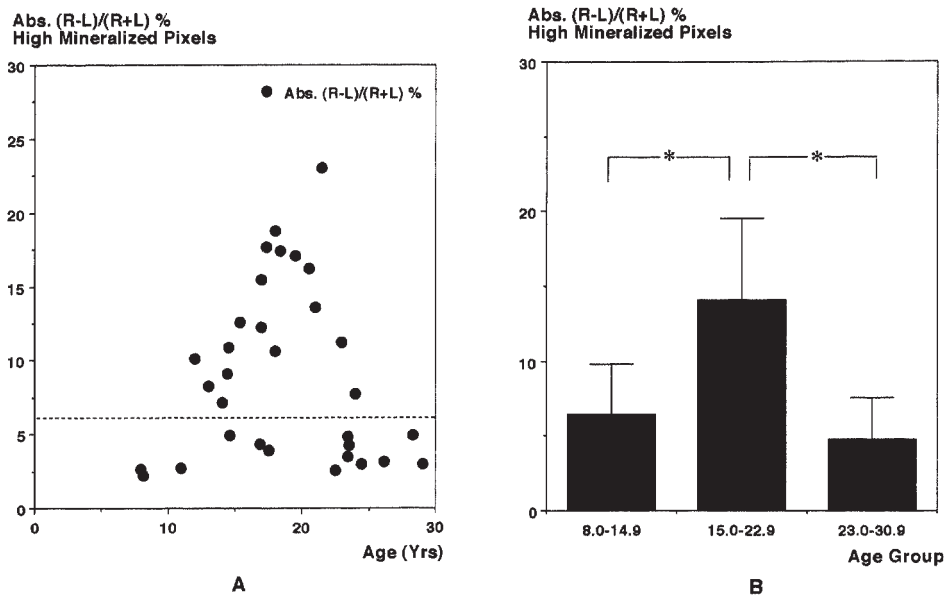


**Figure 8** The percentage difference in the number of pixels with highest mineralized cortical bone is compared with age. (A) The percentage difference (R – L/R + L)% is plotted against the age of each of the 32 subjects with asymmetrical mandibles. The mean (dotted horizontal line) for the percentage difference among 32 subjects with symmetrical mandibles is shown for comparison. (B) The mean ± 1SD for the percentage difference is determined for the asymmetrical subjects in three age ranges. * Indicates statistically significant differences based on a single factorial ANOVA, $P < 0.05$.

comparing them with the left masseter and medial pterygoid (RM + RMPt/LM + LMPt, Figure 9A) indicated a moderately positive correlation ($r$ = 0.418) to the asymmetrical distribution of the highest mineralized cortical bone between the left and right sides of the mandible. The highest correlation coefficient (Figure 9B, $r$ = 0.658) occurred when the ipsilateral masseter muscle and contralateral medial pterygoid muscles were combined.

*Crossbite analysis*

Subjects with asymmetrical mandibles demonstrated a high percentage of crossbites (Figure 10). Crossbites occurred bilaterally in 22 per cent of the subjects. Unilateral crossbites occurred on more on the short (40 per cent) side than the long (13 per cent) mandibular side. A few subjects demonstrated anterior crossbites (3 per cent). Crossbites were determined by taking successive coronal views through the mandible and using the threshold of mineralization to denote the tooth enamel (Figure 11).

## Discussion

*Mineralization of cortical bone*

This is the first study that has evaluated the distribution of mineralized cortical bone in a 3D reconstructed asymmetrical mandible. The main focus of this investigation was on the highest mineralized bone as it is assumed to be pure cortical bone of the mandible. We believe that the highest mineralized cortical bone relates to the densely compacted cortical bone defined histologically. A first study in subjects with symmetrical mandibles has shown that the highest mineralized regions occupy the mandibular corpus and the lower anterior border of the ramus. Other patterns of distribution emerge later and include a wider region of the midramus. This bilateral symmetrical pattern of bone

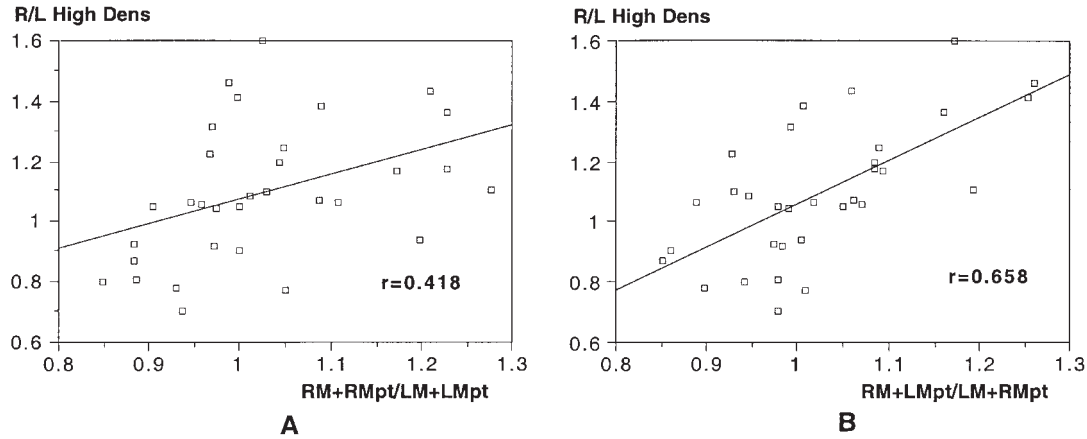


**Figure 9** The ratio between the right and left sides in the number of pixels with the highest mineralized bone (R/L High Dens) is compared with the ratio of the cross-sectional area of the bilateral muscles by linear regression. (A) The right muscles composed of the right masseter (RM) and medial pterygoid (RMPt) are compared to the left muscles (LM + LMPt). (B) The combination of the right masseter and left medial pterygoid (RM + LMpt) is compared to that of the left masseter and right medial pterygoid (LM + RMpt).

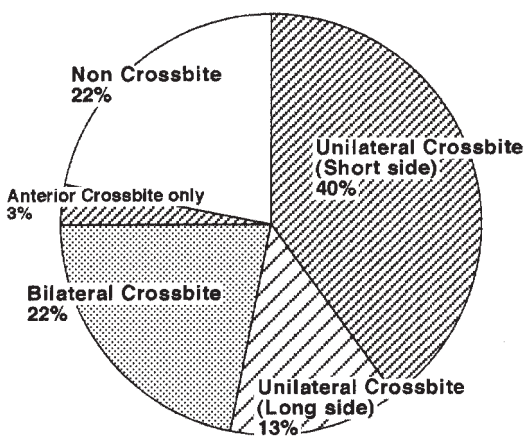


**Figure 10** The percentage of subjects demonstrating occlusal crossbites is shown. Crossbites were determined by evaluating successive coronal views of the 3D reconstructed mandible. Seventy-eight per cent of the subjects demonstrated some form of crossbite.

mineralization in the human mandible agrees with findings in the rhesus monkey (Miller *et al.*, 1988).

It is assumed that among the factors that effect mineralization of the cortical bone are the jaw and facial muscles. Studies in the subjects with symmetrical mandibles indicate a high correlation between muscle cross-sectional area and increased mineralization of the mandible. This finding suggests that the mandible increases mineralization associated with potentially greater forces developed by the jaw-closing muscles (e.g. masseter). It is presumed that subjects demonstrating the minimal distribution of the highest mineralization (e.g. in the body of the mandible and along the anterior border of the ramus) are those that develop the weakest muscles forces. The tension developed by a muscle is directly related to its cross-sectional area. The vector and direction of this force, which change during postnatal development, may be additional muscle characteristics that determine the mineralization. The size and direction of forces developed by at least three mandibular muscles (i.e. temporalis, masseter, and medial pterygoid) are considered the important factors. These muscles can twist, bend, compress, and stretch the mandible, as well as apply shear strain, and must do this within a certain level of energy to signal bone cellular activity (Hatcher *et al.*, 1997a,b).

The few studies that have evaluated muscle use and force with mineralization of skeletal bones indicate a long lag period of 1–2 years before bone demonstrates changes in cortical bone mineralization (Sievanen *et al.*, 1996). These findings suggest that the muscle function must remain above a threshold level for an extended

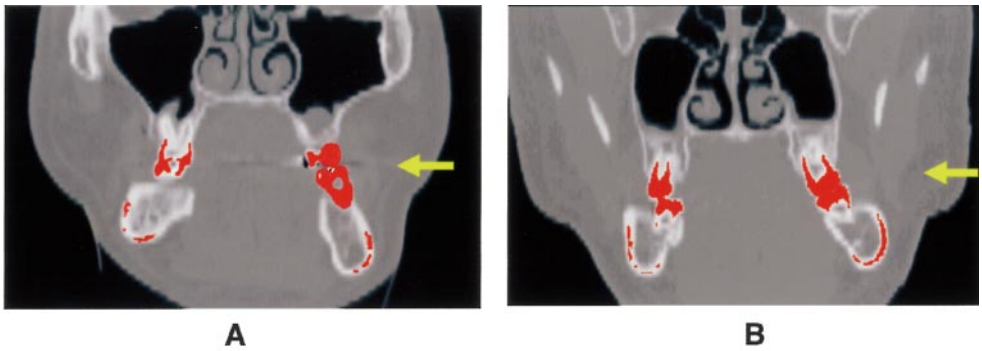


**Figure 11** An example of a coronal view through the 3D reconstructed mandible. The section through the first molar is evaluated by depicting the highest mineralized regions to include the tooth enamel to define the tooth. (A) Example of a crossbite (yellow arrow) on the left and short side of one patient's mandible. (B) Example of a crossbite on the left side that is also the long side of the mandible. Subjects exhibit complex interactions of both dental arches that extend beyond the simple classification of crossbites.

period before the mineralization pattern emerges. It is conjectured that the highest mineralized regions depend on a long-term repeated pattern of recruitment of the muscle as would be evident in a particular chewing pattern or incisal function. It is believed that the distribution of bone mineralization demonstrates the history of mechanical effects on the mandible, and that this distribution changes during growth and development. While cephalometric evaluations can indicate changes in mandibular shape and size, measurements of mineralization distribution may provide more accurate information on how jaw muscles load and affect the bone.

Studies involving monkeys and rabbits have attempted to evaluate a possible cause-effect relationship that would complement work in humans. In the first monkey model, the mandibular occlusion was altered by the permanent placement of a full-occlusion metallic cobalt-chromium splint with a lateral incline (Curtis *et al.*, 1991; Miller, 1991). Each time the animal closed into occlusion, the mandible shifted to the left. After 3 months of wear, the CT-generated material indicated an increased density of bone within the right coronoid and both necks of the condyles, and the development of an asymmetrical distribution of cortical bone density in the upper ramus and zygomatic arch. In a second monkey model, only one mandibular muscle (i.e. left temporalis muscle) was continually stimulated to periodically contract at low levels and the resulting effect on the mineralized cortical bone in the mandible was evaluated (Miller, 1991; Karkhanehchi *et al.*, 1996). The low-level contraction occurred 24 hours/day for 2–12 months and just perceptibly induced a minimal raising of the jaw at a low frequency of 5-Hz or with brief 30-Hz trains. This relatively low, but consistent contraction of the left temporalis induced an asymmetrical change in the bone density, and increased the area of most mineralized bone within the ipsilateral upper ramus and condyle as compared with the contralateral side. The third animal model involved altering the resting posture in the rapidly growing rabbit (Kapila *et al.*, 1990). Miniature magnets were glued to the upper and lower anterior incisors, and the poles orientated to shift the mandible only when the rabbit was at rest. Recruitment of jaw muscles as during chewing would correct this laterally situated resting mandibular posture. Evaluation of CT images indicated a shift in the bone mineral density to an asymmetrical bilateral pattern in the zygomatic arches. These animal studies demonstrate that cortical bone mineralization can become asymmetrical when inducing changes in bilateral recruitment patterns of jaw muscles.

In this present study, it has been shown that mineralization of the mandibular cortical bone is dynamic, demonstrating its most asymmetrical patterns between the left and right mandibular sides during the growth period of the subjects (e.g. 15–23 years). Intriguingly, after full development of the asymmetrical mandible at the completion of the growth period, the asymmetrical distribution of the highest mineralized areas of cortical bone decreases to the normal range. It appears that the mandibular cortical bone with the highest mineralized tissue occupies a similar amount of cortical bone bilaterally within a fully developed asymmetrical structure. This finding may suggest that the craniomandibular muscles develop an equilibrium with the asymmetrical skeleton in which relatively similar bilateral forces are generated in the nonsymmetrical bilateral bone. This concept will need to be tested in a larger number of subjects with a more complex evaluation of function and the forces it generates within the cranioskeleton. The original assumption was that a developing asymmetrical mandible would be associated with chewing and other functions favouring one side. However, after full development of this asymmetrical structure, the muscles in oral function may provide a more balenced set of bilateral forces. This concept will need to be tested.

*Mandibular asymmetries*

The subjects in this study have parents with normal symmetrical mandibles and were born with symmetrical mandibles. A previous review of mandibular asymmetry has shown that investigators need to distinguish between apparent asymmetrical mandibles and true asymmetry (Hatcher *et al*., 1997a,b). This study indicated that jaw asymmetries are clinical signs of a range of pathological conditions. True mandibular asymmetries occur when either one side is too large or one side is too small (Burke, 1992; Miller *et al*., 1994; Westesson *et al*., 1994). The aetiology of a true asymmetry usually occurs with a small condyle and ipsilateral mandibular side. Based on Pirttiniemi's review (1994), the more recent approaches to dividing the heterogeneous group of craniomandibular asymmetries relates to the onset of the defect instead of the cause (van der Meulen *et al*., 1983; Stricker *et al*., 1990). Mandibular asymmetries appear in the embryonic (i.e. hemifacial microsomia), foetal, and postnatal periods. The smallest number of clinical cases relates to the congenital conditions evident in the embryonic and foetal stages (Hatcher *et al*., 1997a,b). The most frequently acquired mandibular asymmetries encountered in clinical practice are due to destructive conditions (i.e. fractures, avascular necrosis, and arthritides that include rheumatoid arthritis and degenerative joint disease) and altered occlusal interactions.

In subjects with mandibular asymmetries with predominantly postnatal expression, several factors are important. Unilateral overgrowth of the mandibular condyle can modify the growth of the entire mandible (Bruce and Hayward, 1968; Matteson *et al*., 1985; Pogrel, 1985; Obwegeser and Makek, 1986; Henderson *et al*., 1990). Some investigators have divided condylar hyperplasia into an idiopathic form that appears during adolescence and a form associated with degenerative and arthrotic changes during adulthood (Slottweg and Muller, 1986). Potential aetiological factors suggested by other investigators include changes in vascularity to one condyle (Oberg *et al*., 1962; Blackwood, 1965), previous trauma to the temporomandibular joint (Jacobsen and Lund, 1972), and certain endocrine disorders (Muller, 1979). There is much less evidence for progressive hemifacial atrophy (Pirttiniemi, 1994). Rarely would rheumatoid arthritis or arthritis affect one joint inducing an asymmetrical mandible. However, mandibular fractures with injury to the condylar region can modify the bilateral growth and distort the mandible in shape and size (Lund, 1974; Proffit *et al*., 1980). In the present investigation, the asymmetry developed as the subjects were older than 8 years. The primary cause of the asymmetry has not been diagnosed, but each of the subjects was referred based on the evident asymmetry appearing later in life.

The subjects in this study with asymmetrical mandibles demonstrate a much higher percentage (78 per cent) of crossbites than normal subjects (5–21 per cent; Larsson, 1986; Kurol and

Berglund, 1992). The relationship of the crossbites to an asymmetrical mandible is a difficult question. One possibility is that some subjects developed crossbites that might induce an asymmetrical mandibular development. Abnormal or habitual patterns of function (i.e. thumb sucking) are potential factors inducing crossbites. However, the highest proportion of crossbites (40 per cent) was found on the short mandibular side. It may be that an independent factor, e.g. trauma to the condyle, induced abnormal development of the mandible and resulted in malocclusions that expressed themselves primarily as crossbites. Such alterations in the articulating surfaces of the dentition and their vector of interdigitation would be expected to alter the recruitment of the mandibular muscles during functions such as chewing and swallowing (Troelstrup and Møller, 1970). Shifting forces on the dentition will also alter the reaction forces on the bilateral condyles and the neck of the condyle (Hatcher *et al*., 1997a,b; Maki *et al*., 1999).

A longitudinal study is needed to evaluate the progression of factors that occur to determine the cause-effect relationships. It is conjectured that the mandibular jaw-closing muscles must alter their function sometime in the progressive development of the mandibular asymmetry, and further enhance the change in direction of forces transmitted through the condyles and mandible. Previous surface electromyographic recordings from subjects that exhibited mild temporomandibular joint involvement (i.e. loss of the condylar cartilage and disc) in a congenital unilateral problem has shown that the masseter is affected more than the temporalis in recruitment (Miller, 1991). The masseter on the unaffected side demonstrates more recruitment during chewing and other jaw movements than in normal subjects, suggesting a shift in the bilateral recruitment patterns of the masseter muscles. The function of jaw muscles is presently being evaluated. It is suspected that the co-activation patterns of the bilaterally positioned jaw muscles are unbalanced and induce the differences in cross-sectional areas of the muscles.

**Address for correspondence**

Professor Arthur J. Miller
Box 0438
Department of Growth and Development
School of Dentistry
University of California at San Francisco
San Francisco
CA 94143
USA

**Acknowledgements**

This work was supported by the Japanese Ministry of Education and was conducted in collaboration with the Departments of Orthodontics at Showa University, the Mechanical Engineering Department at the Tokyo Institute of Technology, and the Department of Orthodontics at the University of California at San Francisco.

**References**

Bentzen S M, Hvid I, Jorgensen J 1987 Mechanical strength of tibial trabecular bone evaluated by x-ray computed tomography. Journal of Biomechanics 20: 743–752

Bhasin S, Sartoris D J, Fellingham L 1988 Three-dimensional quantitative CT of the proximal femur: relationship to vertebral trabecular bone density in postmenopausal women. Radiology 167: 145–149

Blackwood H J J 1965 Vascularization of the condylar cartilage of the human mandible. Journal of Anatomy 99: 551–563

Bouvier M, Hylander W L 1996 The mechanical or metabolic function of secondary osteonal bone in the monkey. Archives of Oral Biology 41: 941–950

Bruce R A, Hayward J R 1968 Condylar hyperplasia and mandibular asymmetry. Journal of Oral and Maxillofacial Surgery 26: 281–290

Burke P 1992 Serial observation of asymmetry in the growing face. British Journal of Orthodontics 19: 273–285

Carter D R, Hayes W C 1976 Bone compressive strength: the influence of density and strain rate. Science 194: 1174–1176

Curtis D A, Nielsen I, Kapila S, Miller A J 1991 Adaptability of the adult primate craniofacial complex to asymmetrical lateral forces. American Journal of Orthodontics and Dentofacial Orthopedics 100: 266–273

Faulkner K G, Cann C E, Hasegawa B H 1991 Effect of bone distribution in vertebral strength assessment with patient-specific non-linear finite element analysis. Radiology 179: 669–674

Hatcher D C, McEvoy S P, Mah R 1997a Maxillomandibular relationships: Mandibular asymmetry, occlusion, and imaging. In: McNeill C M (ed.) Science and practice of occlusion. Quintessence Publishing Co, Chicago, pp. 273–293

Hatcher D C, McEvoy S P, Mah R T, Faulkner M G 1997b Distribution of local and general stresses in the stomatognathic system. In: McNeill C M (ed.) Science and practice of occlusion. Quintessence Publishing Co, Chicago, pp. 259–270

Henderson M J, Wastie M L, Bromige M, Selwyn P, Smith A 1990 Technetium-99m bone scintigraphy and mandibular condylar hyperplasia. Clinical Radiology 41: 411–414

Jacobsen P U, Lund K 1972 Unilateral overgrowth and remodeling processes after fracture of the mandibular condyle. Scandinavian Journal of Dental Research 80: 68–74

Kapila S, Miller A, Curtis D, Hatcher D 1990 Effect of lateral deviation of mandibular position on craniomandibular growth. Journal of Dental Research 69: 339 (abstract)

Karkhanehchi J, Maki M, Faria M, Curtis D, Miller A 1996 Cortical bone mineral density of the rhesus monkey craniofacial skeleton. Journal of Dental Research 75: 309 (abstract)

Korioth T W P, Romilly D P, Hannam A G 1992 Three-dimensional finite element stress analysis of the dentate human mandible. American Journal of Physical Anthropology 88: 69–96

Kurol J, Berglund L 1992 Longitudinal study and cost-benefit analysis of the effect of early treatment of posterior cross-bites in the primary dentition. European Journal of Orthodontics 14: 173–179

Larsson E 1986 The effect of dummy-sucking on the occlusion: a review. European Journal of Orthodontics 8: 127–130

Lund K 1974 Mandibular growth and remodeling process after condylar fracture. A longitudinal roentgencephalometric study. Acta Odontologica Scandinavica 32 (Supplement 64)

Maki K, Shibasaki Y, Fukuhara T 1989 A new approach for mandibular growth by X-ray CT. Dentistry in Japan 26: 77–80

Maki K, Okano T, Morohashi T, Yamada S, Shibasaki Y 1997 The application of 3D quantitative computed tomography to the maxillofacial skeleton. Journal of Dental and Maxillofacial Radiology 26: 39–44

Maki K, Inou N, Miller A, Shibasaki Y 1999 Computer-assisted systems to evaluate jaw loading and movement. Journal of Dental Research 78: 528 (abstract)

Maki K, Miller A J, Okano T, Shibasaki Y 2000 Changes in cortical bone mineralization in the developing mandible: a 3D quantitative computed tomography study. Journal of Bone and Mineral Research (in press)

Matteson S R, Proffit W R, Terry B C 1985 Bone scanning with 99m technetium phosphate to assess condylar hyperplasia. Oral Surgery, Oral Medicine, Oral Pathology 60: 356–367

Miller A 1991 Craniomandibular muscles: their role in function and form. CRC Press, Boca Raton, pp. 246–253

Miller A J, Cann C E, Nielsen I L, Roda G 1988 Craniomandibular bone density in the primate as assessed by computed tomography. American Journal of Orthodontics and Dentofacial Orthopedics 93: 117–125

Miller V, Myers S, Yoeli Z, Zeltzer C 1994 Condylar asymmetry and its relation to age in a group of patients with a craniomandibular disorder of myogenous origin. Journal of Oral Rehabilitation 21: 707–711

Moss M L, Skalak R, Patel H, Sen K, Moss-Salentijn L, Shinozuka M 1985 Finite element method modeling of craniofacial growth. American Journal of Orthodontics 87: 453–472

Muller H 1979 Unilateral condylar hyperplasia and acromegaly. Journal of Maxillofacial Surgery 7: 73–76

Oberg T, Fajers C M, Lysell G, Friberg U 1962 Unilateral hyperplasia of mandibular condylar process. Acta Odontologica Scandinavica 20: 485–504

Obwegeser H L, Makek M S 1986 Hemimandibular hyperplasia-hemimandibular elongation. Journal of Maxillofacial Surgery 14: 183–208

Pirttiniemi P M 1994 Associations of mandibular and facial asymmetries—a review. American Journal of Orthodontics and Dentofacial Orthopedics 106: 191–200

Pogrel M A 1985 Quantitative assessment of isotope activity in the temporomandibular joint regions as a means of assessing unilateral condylar hypertrophy. Oral Surgery, Oral Medicine, Oral Pathology 60: 15–17

Proffit W R, Vig K W L, Turvey T A 1980 Early fracture of the mandibular condyles: frequently an unsuspected cause of growth disturbances. American Journal of Orthodontics 78: 1–24

Ruegsegger P, Steiger P, Felder M 1988 Quantitative computed tomography of the rheumatic knee. Clinical Rheumatology 7: 486–491

Sievanen H, Heinonen A, Kannus P 1996 Adaptation of bone to altered loading environment: a biomechanical approach using X-ray absorptiometric data from the patella of a young woman. Bone 19: 55–59

Slottweg P J, Muller H 1986 A clinicopathological analysis of 22 cases. Journal of Maxillofacial Surgery 14: 209–214

Stricker M, van der Meulen J C, Raphael B, Mezzola R, Tolhurst D E, Murray J E (eds) 1990 Craniofacial malformations. Churchill-Livingstone, London

Troelstrup B, Møller E 1970 Electromyography of the temporalis and masseter muscles in children with unilateral cross-bite. Scandinavian Journal of Dental Research 78: 425–430

van der Meulen J C, Mazzola R, Vermey-Deerrs C, Stricker M, Raphael B 1983 A morphogenetic classification of craniofacial malformations. Plastic and Reconstructive Surgery 71: 560–572

Westesson P-L, Tallents R, Katzberg R, Guay J A 1994 Radiographic assessment of asymmetry of the mandible. American Journal of Neuroradiology 15: 991–999